Density functional study of Li_4NH and $Li_{1.5}NH_{1.5}$ as intermediary compounds during hydrogenation of Li_3N

J.-C. Crivello,[1,*] M. Gupta,[2] R. Černý,[3] M. Latroche,[1] and D. Chandra[4]
[1]*Chimie Métallurgique des Terres Rares, ICMPE, UMR 7182, CNRS, 2-8 rue H. Dunant, 94320 Thiais, France*
[2]*Thermodynamique et Physico-Chimie d'Hydrures et Oxydes, Université de Paris Sud, 91405 Orsay, France*
[3]*Laboratory of Crystallography, University of Geneva, 24 quai Ernest-Ansermet, CH-1211 Geneva 4, Switzerland*
[4]*Chemical and Metallurgical Engineering Faculty, University of Nevada, Reno, Nevada 89557 USA*
(Received 29 November 2009; revised manuscript received 2 February 2010; published 26 March 2010)

Recent experimental data suggest the formation of two new compounds, namely, Li_4NH and $Li_{1.5}NH_{1.5}$, during the hydrogenation process of Li_3N. The formation of these compounds could modify the hydrogen absorption and desorption characteristics of Li_3N. We present here the results of our density functional theory calculations concerning their formation. We find that the direct hydrogenation reaction of Li_3N to Li_2NH is predominantly favored but the formation of Li_4NH is possible through the direct formation involving Li_3N and LiH with an enthalpy of reaction much less negative than for the direct formation of Li_2NH. The formation of this compound through the release of ammonia is not possible. This compound readily reacts with H_2 exothermically with an enthalpy of reaction less negative than for the direct process. We also find that the formation of the intermediate phase $Li_{2-x}NH_{1+x}$ for $x=0.5$ between imide ($x=0$) and amide ($x=1$) is possible. $Li_{1.5}NH_{1.5}$ is found to form in a cubic Li-vacant-type compound. After full relaxations of several structural models, the $Li_{1.5}NH_{1.5}$ compound presents a coexistence of ordered $[NH]^{2-}$ and $[NH_2]^-$ anions. These results are discussed in terms of an analysis of the electronic structures of these compounds.

DOI: 10.1103/PhysRevB.81.104113 PACS number(s): 71.15.Nc, 71.20.Nr, 61.50.Lt, 61.50.Ah

I. INTRODUCTION

There is considerable interest in hydrogen as a clean fuel and this has lead to intense effort for its storage in solid matrices in the form of hydrides which is safe and reversible. Significant amount of work has been performed over the last decades on intermetallic compounds,[1,2] currently classified as "Classical Hydrides." These materials can usually absorb hydrogen reversibly by formation of metallic hydrides, where H atoms occupy interstitial sites in the host matrix. From these investigations, a large number of compounds have emerged with optimum properties for several specific applications.[3–5] Although the volumetric capacity for hydrogen storage in these compounds is very high, nearly twice as much as liquid hydrogen, their weight percent capacity is quite low, about few weight percent for the best-studied intermetallic compound and this has limited their portable applications. Attention has therefore turned toward low-weight "Complex (Chemical) Hydrides" such as alanates[6] or borohydrides[7] as potential candidates for advanced hydrogen storage materials due to their high gravimetric densities even if their complete integration in industrial applications is still very far due to reversibility problems, cost of production, high temperatures of desorption, and safety issues.

The hydrogenation properties of the light-weight compound, Li_3N have been thoroughly investigated following the work of Chen *et al.*[8–11] These authors showed that the chemical reaction proceeds via the two following steps and leads to the theoretical capacity of 10.2 wt % hydrogen,

$$Li_3N + H_2 \Leftrightarrow Li_2NH + LiH \quad (1)$$

$$Li_2NH + H_2 \Leftrightarrow LiNH_2 + LiH. \quad (2)$$

While the enthalpy of the first reaction is highly exothermic, ~ -161 kJ mol^{-1} H_2,[8] and thus requires very high temperatures to release hydrogen, the heat of the second reaction, derived from the van't Hoff plots[8,12,13] is more favorable for applications, varying between −45 and −51 kJ mol^{-1} H_2. The temperature of desorption remains still high and the weight capacity for this reaction drops to 6.4 wt %.

Recently, it has been suggested that the reaction pathways might be more complex than suggested by Eqs. (1) and (2) since, first the formation of a new compound Li_4NH has been detected,[14] and second the consumption of Li_3N is higher than suggested by Eq. (1). Further, David *et al.*[15] have also suggested the formation of a series of nonstoichiometric phases with the composition $Li_{2-x}NH_{1+x}$. Indeed, both Li_2NH and $LiNH_2$ are the end members of this series with values of $x=0.0$ and $x=1.0$, respectively. Chandra *et al.*,[16] in a recent investigation of the phase diagram Li_3N-H_2 observed also that the hydrogenation of Li_3N proceeds along more complex reactions than Eqs. (1) and (2), and involves, in particular, two intermediary phases: Li_4NH (Ref. 17) and a novel compound $Li_{1.5}NH_{1.5}$ ($x=0.5$).

The mechanisms of the formation of these new phases is clearly important for a proper understanding of the hydrogenation properties of Li_3N. The density functional theory (DFT) based calculations have yielded[18–25] very reasonable enthalpies of formation of many hydrogen storage materials. We have therefore used the DFT calculations to understand the energetics of formation of these new phases, and the results are presented in this paper. Computational details are given in Sec. II. In Sec. III, the crystal structure data for two new phases, namely, Li_4NH and $Li_{1.5}NH_{1.5}$ will be described. The principal features of the electronic structure and hydrogen bonding are discussed in Sec. IV, and in Sec. V, reaction

 ©2010 The American Physical Society

enthalpies are given. The concluding remarks are summarized in Sec. VI.

II. COMPUTATIONAL DETAILS

The DFT calculations[26] were carried out using the Vienna *ab initio* simulation package (VASP).[27,28] The generalized gradient approximation is used for the exchange and correlation energy functionals with the Perdew-Wang (PW91),[29] Perdew-Burke-Ernzerhof (PBE),[30] and the PBE revised for solids (PBEsol)[31] functionals. The choice of three functionals allows us to appreciate the uncertainties that might occur due to the choice of the functional. An energy cutoff of 1000 eV was used for the plane-wave basis set, and a dense grid of k points in the irreducible wedge of the Brillouin zone (k-point spacing less than 0.05 $Å^{-1}$ in each direction) was used with the sampling generated by the Monkhorst-Pack procedure.[32] Both the internal atomic coordinates and the lattice parameters were fully relaxed. For all compounds, relaxations were performed so that the convergence of Hellmann-Feynman forces was better than 1 meV $Å^{-1}$. The self-consistent total-energy calculations converged to less than 0.1 meV. The densities of states (DOS) were obtained using the linear tetrahedron method with Blöchl corrections on relaxed structures.[33] Only the electronic contributions to the heats of formation and reaction are included at 0 K in the present calculations. The contributions from zero-point energies (ZPEs) of the H atoms were estimated within the Einstein model since the major contribution comes from the high-frequency phonons. The trends found in the present estimations are similar to these obtained from full phonon calculations.[24] The charge distribution on the atoms was investigated using Bader's topological analysis.[34] In this approach, atomic charges are calculated using the decomposition of electronic charge density into atomic contributions by dividing the space into atomic regions with surfaces at a minimum in the charge density. We have used the "Bader" code developed by Henkelman *et al.*[35,36]

III. CRYSTAL STRUCTURES

Figure 1 shows the crystal structure of the compounds involved in reactions (1) and (2) and studied in the present work. Whereas the crystal structure of the lithium amide $LiNH_2$ is well known to be described in space group $I\bar{4}$ (No. 82) (Refs. 38 and 39) with an ordering of the NH_2 entities, the crystal structure of the lithium imide Li_2NH is still controversial both from experimental[37,40,41] and theoretical investigations.[21,22,25] This compound appears to present a disordered arrangement of hydrogen atoms depending on the temperature. Following our previous calculation,[23] we used two models for describing Li_2NH, a starting model in the cubic $F\bar{4}3m$ space group (No. 216), as observed at room temperature by neutron powder diffraction of Ohoyama *et al.*,[37] and the orthorhombic *Pnma* space group (No. 62), predicted as the lowest-energy structure by Magyari-Köpe *et al.*[22] The calculated crystal structure data with the three functionals, including the internal atomic coordinates, for the relevant structures are summarized in Table I, where they are

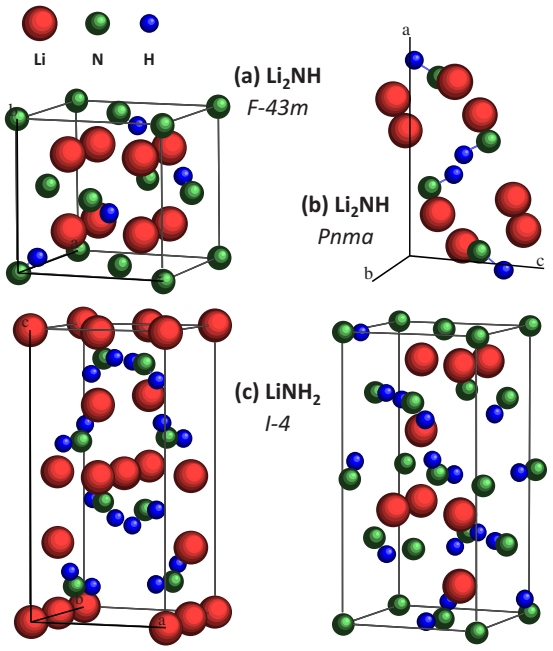

FIG. 1. (Color online) Crystal structures of Li_2NH in (a) $F\bar{4}3m$ (Ref. 37), (b) *Pnma* (Ref. 22), and (c) $LiNH_2$ $I\bar{4}$ (Ref. 38) with two different origins.

compared with the experimental data. The theoretical results are in excellent agreement with the available experimental data, and are not too sensitive to the choice of the functional. Our calculations confirm, as found by Magyari-Köpe *et al.*,[22] that the orthorhombic *Pnma* structure of Li_2NH is more stable than the cubic $F\bar{4}3m$ one at 0 K, and that the relative alignment and ordering of N-H dimmers leads to the lowest-energy state.

We now focus on the crystal structures of the two new intermediate phases represented in Fig. 2. The initial structural parameters for Li_4NH were taken from the x-ray diffraction data of Niewa *et al.*[17] in the tetragonal space group $I4_1/a$ (No. 88). In this structure, the Li atoms occupy the 16f sites while the N and H atoms occupy the 4a and 4b sites, respectively. The lattice parameters and the internal atomic coordinates were fully relaxed starting from these experimental values. Our calculated crystal structure is given in Table I together with the experimental data. The agreement is excellent. In fact, our calculations confirm the validity of a deformation variant of an ordered Li_2O-type superstructure[17,44] and show that in the most favorable structural configuration, N and H atoms occupy uniquely either the 4a or the 4b positions but not both at the same time. For example, if half of the N atoms occupy the 4a sites and the other half the 4b sites (with a similar distribution for the H atoms), the energy is less negative by 144 meV/f.u. After full relaxation, the Li atoms have a distorted configuration. The H atoms are located at tetrahedral interstitial sites surrounded by four Li atoms as first neighbors at a distance of 1.93 Å while the N atoms are surrounded by 8 Li atoms at an average distance of 2.05 Å. This arrangement is drastically different from the one found either in imide or amide where strong interactions between H and N atoms are observed.

TABLE I. Structural parameters of Li-N-H compounds from the present calculations. Experimental values for Li_3N (Ref. 42), LiH (Ref. 43), Li_2NH (Ref. 37), $LiNH_2$ (Ref. 38), and Li_4NH (Ref. 17) are indicated as a comparison, except for Li_2NH calculated in the predicted *Pnma* space group (Ref. 22).

			Experimental			Calculated PW91			Calculated PBE			Calculated PBEsol		
	At.	Wy.	x	y	z	x	y	z	x	y	z	x	y	z
Li_3N (Ref. 42)	Li	1*b*	0	0	$\frac{1}{2}$	0	0	$\frac{1}{2}$	0	0	$\frac{1}{2}$	0	0	$\frac{1}{2}$
*P*6/*mmm* (191)	Li	2*c*	$\frac{1}{3}$	$\frac{2}{3}$	0	$\frac{1}{3}$	$\frac{2}{3}$	0	$\frac{1}{3}$	$\frac{2}{3}$	0	$\frac{1}{3}$	$\frac{2}{3}$	0
	N	1*a*	0	0	0	0	0	0	0	0	0	0	0	0
			a=3.648 Å			a=3.642 Å			a=3.642 Å			a=3.620 Å		
			c=3.875 Å			c=3.878 Å			c=3.875 Å			c=3.861 Å		
			V=44.659 Å^3			V=44.541 Å^3			V=44.501 Å^3			V=43.812 Å^3		
LiH (Ref. 43)	Li	4*a*	0	0	0	0	0	0	0	0	0	0	0	0
$Fm\bar{3}m$ (225)	H	4*b*	$\frac{1}{2}$	$\frac{1}{2}$	$\frac{1}{2}$	$\frac{1}{2}$	$\frac{1}{2}$	$\frac{1}{2}$	$\frac{1}{2}$	$\frac{1}{2}$	$\frac{1}{2}$	$\frac{1}{2}$	$\frac{1}{2}$	$\frac{1}{2}$
			a=4.064 Å			a=4.013 Å			a=4.015 Å			a=3.993 Å		
			V=67.121 Å^3			V=64.611 Å^3			V=64.735 Å^3			V=63.671 Å^3		
Li_2NH (Ref. 37)	Li	4*c*	$\frac{1}{4}$	$\frac{1}{4}$	$\frac{1}{4}$	0.312	0.312	0.312	0.313	0.313	0.313	0.314	0.314	0.314
$F\bar{4}3m$ (216)	Li	4*d*	$\frac{3}{4}$	$\frac{3}{4}$	$\frac{3}{4}$	0.774	0.774	0.774	0.777	0.777	0.777	0.774	0.774	0.774
	N	4*a*	0	0	0	0	0	0	0	0	0	0	0	0
	H	48*h*	0.093	0.093	0.093	0.115	0.115	0.115	0.114	0.114	0.114	0.118	0.118	0.118
			a=5.077 Å			a=5.159 Å			a=5.223 Å			a=5.074 Å		
			V=130.864 Å^3			V=137.334 Å^3			V=142.499 Å^3			V=130.625 Å^3		
Li_2NH (Ref. 22)	Li	4*c*	0.102	$\frac{1}{4}$	0.464	0.102	$\frac{1}{4}$	0.463	0.102	$\frac{1}{4}$	0.463	0.102	$\frac{1}{4}$	0.463
Pnma (62)	Li	4*c*	0.201	$\frac{1}{4}$	0.914	0.201	$\frac{1}{4}$	0.913	0.201	$\frac{1}{4}$	0.913	0.202	$\frac{1}{4}$	0.914
	N	4*c*	0.354	$\frac{1}{4}$	0.218	0.353	$\frac{1}{4}$	0.218	0.353	$\frac{1}{4}$	0.218	0.353	$\frac{1}{4}$	0.218
	H	4*c*	0.424	$\frac{1}{4}$	0.399	0.423	$\frac{1}{4}$	0.398	0.423	$\frac{1}{4}$	0.400	0.432	$\frac{1}{4}$	0.400
			a=7.733 Å			a=7.742 Å			a=7.753 Å			a=7.775 Å		
			b=3.60 Å			b=3.604 Å			b=3.609 Å			b=3.618 Å		
			c=4.872 Å			c=4.883 Å			c=4.890 Å			c=4.881 Å		
			V=135.632 Å^3			V=136.258 Å^3			V=136.839 Å^3			V=137.296 Å^3		
$LiNH_2$ (Ref. 38)	Li	2*a*	0	0	0	0	0	0	0	0	0	0	0	0
$I\bar{4}$ (82)	Li	2*c*	0	$\frac{1}{2}$	$\frac{1}{4}$	0	$\frac{1}{2}$	$\frac{1}{4}$	0	$\frac{1}{2}$	$\frac{1}{4}$	0	$\frac{1}{2}$	$\frac{1}{4}$
	Li	4*f*	0	$\frac{1}{2}$	0.001	0	$\frac{1}{2}$	0.008	0	$\frac{1}{2}$	0.008	0	$\frac{1}{2}$	0.007
	N	8*g*	0.230	0.247	0.115	0.229	0.245	0.115	0.228	0.246	0.115	0.232	0.245	0.116
	H	8g_1	0.226	0.133	0.190	0.227	0.112	0.189	0.226	0.113	0.190	0.229	0.107	0.192
	H	8g_2	0.394	0.349	0.125	0.412	0.334	0.125	0.411	0.334	0.124	0.420	0.333	0.125
			a=5.032 Å			a=5.015 Å			a=5.035 Å			a=4.934 Å		
			c=10.256 Å			c=10.472 Å			c=10.453 Å			c=10.274 Å		
			V=259.692 Å^3			V=263.400 Å^3			V=264.956 Å^3			V=250.074 Å^3		
Li_4NH (Ref. 17)	Li	16*f*	0.194	0.044	0.782	0.189	0.044	0.784	0.191	0.043	0.783	0.190	0.044	0.784
I_{4_1}/a (88)	N	4*b*	0	$\frac{1}{4}$	$\frac{5}{8}$	0	$\frac{1}{4}$	$\frac{5}{8}$	0	$\frac{1}{4}$	$\frac{5}{8}$	0	$\frac{1}{4}$	$\frac{5}{8}$
	H	4*a*	0	$\frac{1}{4}$	$\frac{1}{8}$	0	$\frac{1}{4}$	$\frac{1}{8}$	0	$\frac{1}{4}$	$\frac{1}{8}$	0	$\frac{1}{4}$	$\frac{1}{8}$
			a=4.8765 Å			a=4.858 Å			a=4.860 Å			a=4.863 Å		
			c=9.877 Å			c=9.918 Å			c=9.920 Å			c=9.915 Å		
			V=234.878 Å^3			V=234.103 Å^3			V=234.293 Å^3			V=234.461 Å^3		

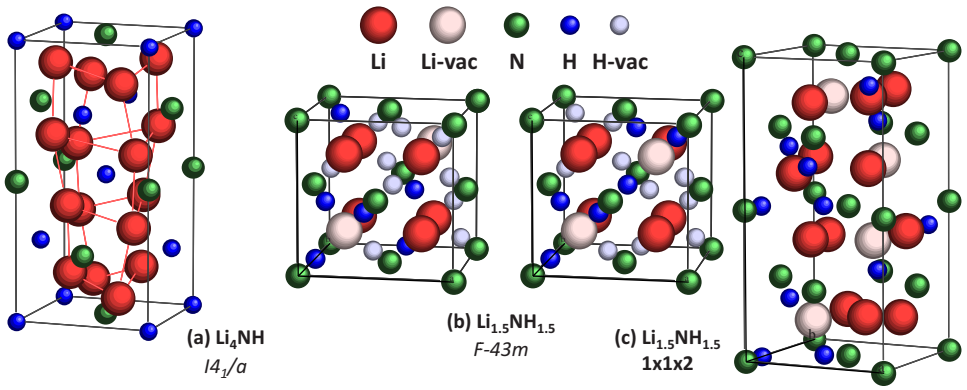

FIG. 2. (Color online) Crystal structures of (a) Li_4NH and two proposed models for $Li_{1.5}NH_{1.5}$, (b) $1\times1\times1$, with Li vacancies located at $\frac{a\sqrt{3}}{2}$, third-nearest neighbor (left) and at $\frac{a\sqrt{2}}{2}$, second-nearest neighbor (right), and (c) a relaxed $1\times1\times2$ supercell model.

X-ray diffraction studies of hydrogen absorption in Li_3N (Ref. 16) show that $Li_{1.5}NH_{1.5}$ phase can be described as a disordered phase derived from the structure of Li_2NH as $Li_{2-x}NH_{1+x}$ with $x=0.5$ between imide ($x=0$) and amide ($x=1$), the structural results are presented in Table II. An homogeneity range ($x=0.25-0.98$) of the Li and H content was observed. The stability of this phase will be discussed in the next section.

As it is mentioned in Ref. 16, the crystal structures of Li_4NH, Li_2NH, $Li_{1.5}NH_{1.5}$, and $LiNH_2$ can be all related to a common antifluoritelike fcc subcell where N, H, NH, and NH_2 anions occupy nodes of the fcc lattice. In the $Li_{1.5}NH_{1.5}$ structure, while the 4*a* sites of N are fully occupied, Li at 4*a* and 4*d* sites have an occupancy of 0.75 and the H 16*e* sites an occupancy of 0.375, which means occupations in a cubic cell calculations of $\frac{6}{8}$ and $\frac{6}{16}$ for Li and H, respectively. Several models were used in theoretical calculations for the ordering of the vacancies at Li and H sites, using $1\times1\times1$ [Fig. 2(b)], $1\times1\times2$ [Fig. 2(c)], and $2\times2\times2$ supercell

TABLE II. $Li_{1.5}NH_{1.5}$ structural results of x-ray powder-diffraction analysis from (Ref. 16), space group $F\bar{4}3m$ (No. 216), isotropic temperature factor B_{iso}(Å^2), and site occupancy (upper part). The most stable calculated structural model of $Li_{1.5}NH_{1.5}$, the initial and fully relaxed positions are given (lower part).

Experimental	At.	Wy.	*x*	*y*	*z*	B_{iso} (Å^2)	Occ.
$a=5.027$ Å	Li	4*c*	$\frac{1}{4}$	$\frac{1}{4}$	$\frac{1}{4}$	1.0	0.75
$V=127.04$ Å^3	Li	4*d*	$\frac{3}{4}$	$\frac{3}{4}$	$\frac{3}{4}$	1.0	0.75
	N	4*a*	0	0	0	1.0	1
	H	16*e*	0.093	0.093	0.093	1.0	0.375
			Initial			Relaxed	
Calculated	At.	*x*	*y*	*z*	*x*	*y*	*z*
$a=5.111$ Å	Li	$\frac{3}{4}$	$\frac{1}{4}$	$\frac{1}{4}$	0.806	0.194	0.329
$V=133.53$ Å^3		$\frac{1}{4}$	$\frac{3}{4}$	$\frac{1}{4}$	0.306	0.694	0.329
		$\frac{1}{4}$	$\frac{3}{4}$	$\frac{3}{4}$	0.227	0.773	0.766
		$\frac{1}{4}$	$\frac{1}{4}$	$\frac{1}{4}$	0.727	0.273	0.766
		$\frac{3}{4}$	$\frac{3}{4}$	$\frac{3}{4}$	0.732	0.768	0.681
		$\frac{1}{4}$	$\frac{1}{4}$	$\frac{3}{4}$	0.232	0.268	0.681
	N	0	0	0	−0.032	0.032	−0.019
		0	0.5	0.5	−0.008	0.508	0.529
		0.5	0	0.5	0.492	0.008	0.529
		0.5	0.5	0	0.468	0.532	−0.019
	H	0.093	0.093	0.093	0.129	0.093	0.087
		0.593	0.593	0.093	0.629	0.593	0.087
		0.907	0.593	0.407	0.908	0.592	0.364
		0.407	0.093	0.407	0.408	0.092	0.364
		0.907	0.907	0.093	0.907	0.871	0.087
		0.407	0.407	0.093	0.407	0.371	0.087

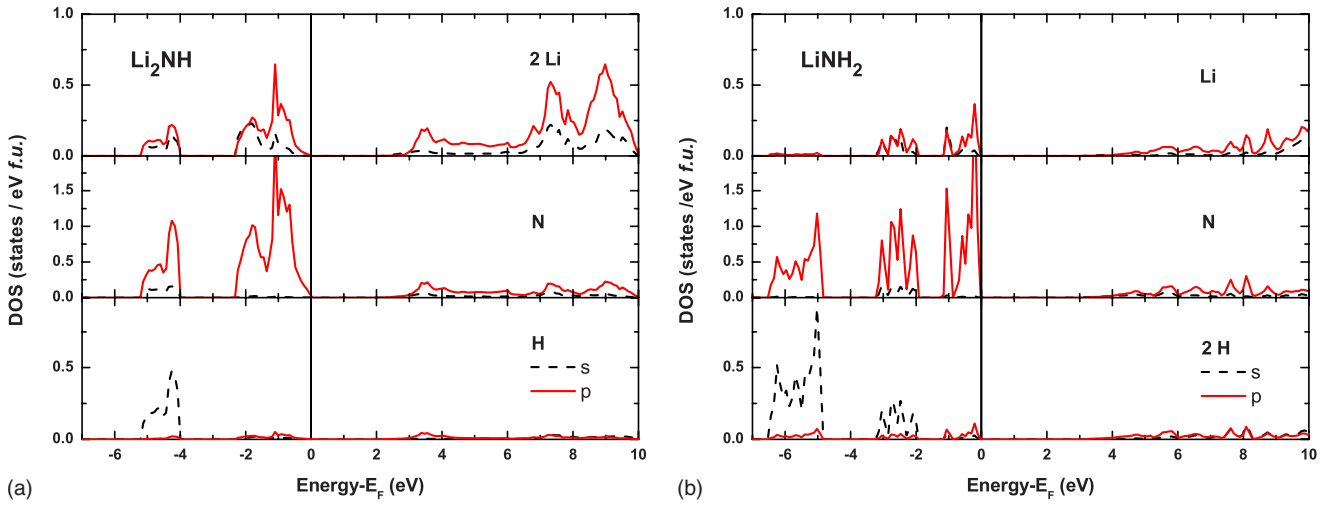

FIG. 3. (Color online) Partial wave analysis of the density of states of (a) Li_2NH in *Pnma* and (b) $LiNH_2$ in $I\bar{4}$ around the atomic sites (*s* states: dashed line and *p* states: full line). The Fermi level is located at the top of valence band and chosen as the origin of energies.

models. After volume and internal coordinate relaxations, the most stable configuration was found to consist of an arrangement in which the Li vacancies are located at $\frac{a\sqrt{2}}{2}$ from each other (second-nearest neighbor), and the H atoms close to the Li vacancies and away from Li atoms to avoid too short Li-H distances. In fact, all configurations with Li vacancies located at $\frac{a}{2}$ (first-nearest neighbor) or at $\frac{a\sqrt{3}}{2}$ [third-nearest neighbor, as an example on Fig. 2(b)] do not lead to a stable ordering of N-H and N-H_2 bonds. In Table II, we give the calculated structural results obtained for the lowest-energy state of $Li_{1.5}NH_{1.5}$. We started with the following configuration of Fig. 2(b): one Li vacancy at each Wyckoff site (4*c*,4*d*) was chosen at $(\frac{1}{4}\frac{1}{4}\frac{1}{4})$ and $(\frac{3}{4}\frac{1}{4}\frac{3}{4})$, one NH_2 entity is located in the corner and other one at an N face center. The remaining two N at the face centers are involved in N-H bonds. After full relaxation, it is remarkable that the NH and NH_2 entities are found to be ordered in the same plane. In the NH_2 entities, the angle is found to be 101.8° and the N-H distances 1.031 Å while the N-H bond length in NH entities is 1.036 Å (results with PW91 functional), which is quite close to the values found in the amide and the imide. Thus in the most stable relaxed structure, half of the nitrogen atoms are involved in N-H bonds and the other half in H-N-H bonds, reflecting the equal mixing of the amide-imide character in this material. Relaxed cubic cell parameter is 5.111 Å, in good agreement with the refined parameter 5.027 Å (Table II). From the DFT optimization at 0 K, this final result of the most stable $Li_{1.5}NH_{1.5}$ structure shows an ordering of Li vacancies and $[NH]^{2-}$ and $[NH_2]^-$ anions which was not, however, observed experimentally in Ref. 16 by x-ray powder diffraction between 300 and 563 K.

IV. RESULTS AND DISCUSSION

A. Electronic structures

The formation of imide and amide are important steps in reaction (1) and (2), we briefly recall the main features of the electronic structure of these compounds, that we found to be in agreement with previous calculations.[19–21,23]

Figure 3 shows the site-projected DOS for (a) the imide Li_2NH and (b) the amide $LiNH_2$. For both compounds, the N 2*s* hybridized with H *s* states localized around −14 eV but are not displayed in Fig. 3. The analysis of the DOS in Fig. 3(a) shows, at energies above −5.5 eV, that the valence band splits into two distinct structures separated by a 1.5 eV energy gap.[23] In Li_2NH, out of the three 2*p* orbitals of N, only the one directed toward H is involved in a strong bonding with hydrogen. The single band associated to this bonding N-H interaction contains two electrons and corresponds to the lowest-energy structure in the DOS. The remaining two N 2*p* orbitals are essentially nonbonding with hydrogen, they correspond to two bands and form the next occupied structure that accommodates four electrons. The three occupied bands associated to the $[NH]^{2-}$ entities are also strongly hybridized with Li *sp* states as it appears clearly in Fig. 3(a).

In the case of $LiNH_2$ [Fig. 3(b)], the valence band splits into three structures, each of them corresponds to one energy band and thus accommodates two electrons. The two N 2*p* orbitals located in the plane of the NH_2 entities interact with the H *s* states while the third N 2*p* orbitals perpendicular to the NH_2 planes are nonbonding with hydrogen. The N 2*p* states are also strongly hybridized with the Li *sp* states. The two materials are insulating with a gap on the order of 3 eV. The empty conduction bands are mainly due to Li *sp* states with a small contribution of antibonding N-H or N-H_2 interactions. The main features of the occupied valence bands, in particular, of their splitting into two and three structures, respectively, for the imide Li_2NH and amide $LiNH_2$ can be simply understood in terms of quasimolecular interactions in the $[NH]^{2-}$, respectively, $[NH_2]^-$ entities.

We now focus on the analysis of the Li_4NH compound. The calculation has been performed in the primitive body-centered tetragonal cell. The electronic band structure of 2 formula-Li_4NH along some high-symmetry directions is shown in Fig. 4. At low energy (−11 eV), two localized bands correspond to N 2*s* states. These are not shown in Fig. 5 in which the total and the partial density of states of Li_4NH

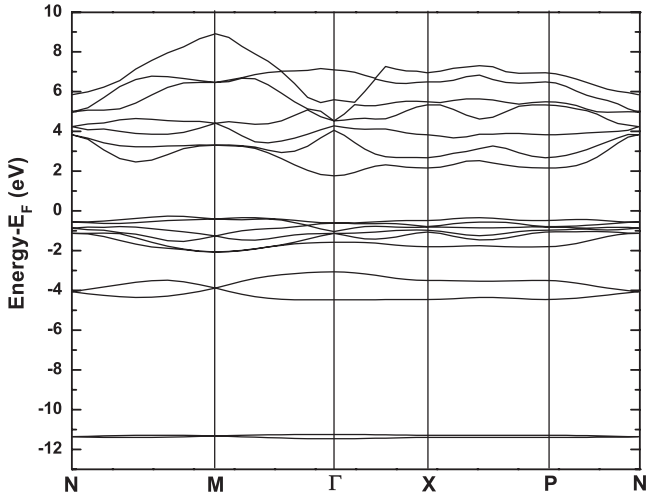

FIG. 4. Band structure of 2 formula-Li_4NH along some high-symmetry directions calculated in the primitive body-centered tetragonal cell.

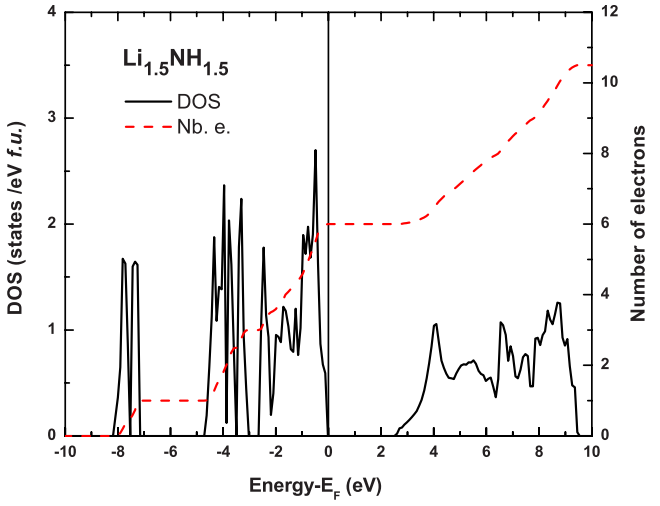

FIG. 6. (Color online) Total density of states (full line, left-hand side scale) and number of electrons (dashed line, right-hand side scale) of $Li_{1.5}NH_{1.5}$.

are plotted. The valence band of Li_4NH, total width ~4.3 eV, splits into two distinct structures. The first one (2 electrons/f.u.) corresponds to the interaction of H *s* state which occurs only with Li *sp* states and not with nitrogen since there is no direct N-H interaction in Li_4NH, as expected from the crystal structure features. The bands plotted in Fig. 4 have a weak dispersion, and the corresponding structure in the DOS is narrow ~1.4 eV. The second structure (6 electrons/f.u.) is associated to the N *p*-Li *sp* interaction. In contrast to the imide and amide, the three N 2*p* bands do not split since there is no direct bonding interaction with H. Consequently, the corresponding structure in the DOS has a narrow width ~1.9 eV. The calculated gap between the valence and the conduction band is about 2.2 eV. The value of the gap is consistent with the reddish color experimentally observed for this compound. The empty conduction bands mostly associated with Li *sp* states have a much larger dispersion than the occupied narrow valence bands.

In the following, we now discuss the electronic structure of the second phase $Li_{1.5}NH_{1.5}$. Figures 6 and 7 display, respectively, the total and partial DOS of $Li_{1.5}NH_{1.5}$. From the analysis of Fig. 7, it is clear that the total contribution of the valence band of $Li_{1.5}NH_{1.5}$ results from the superposition of a two peak structure due to the N-H bonding and from a three-peak structure of the DOS, associated to the bonding of $[NH_2]^-$ entities. Such features have been discussed previously for the imide Li_2NH and the amide $LiNH_2$. It is remarkable that this compound behaves as an intermediary between the two compounds since it presents bonding features of both the imide and the amide in equal proportion.

B. Charges density and partial ordering

In Table III, we give the ionic radii and the charge distribution of all relaxed structures of each entity. For Li_3N, LiH,

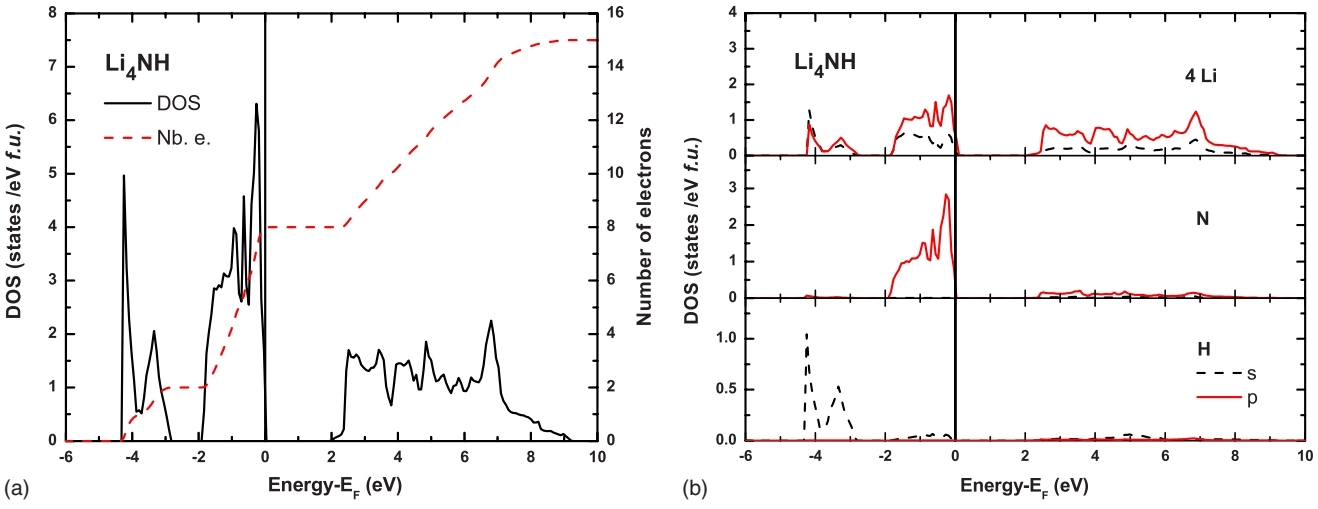

FIG. 5. (Color online) (a) Total density of states (full line, left-hand side scale) and number of electrons (dashed line, right-hand side scale), and (b) partial wave analysis of the density of states around the atomic sites of Li_4NH in $I4_1/a$. The Fermi level is located at the top of valence band and chosen as the origin of energies.

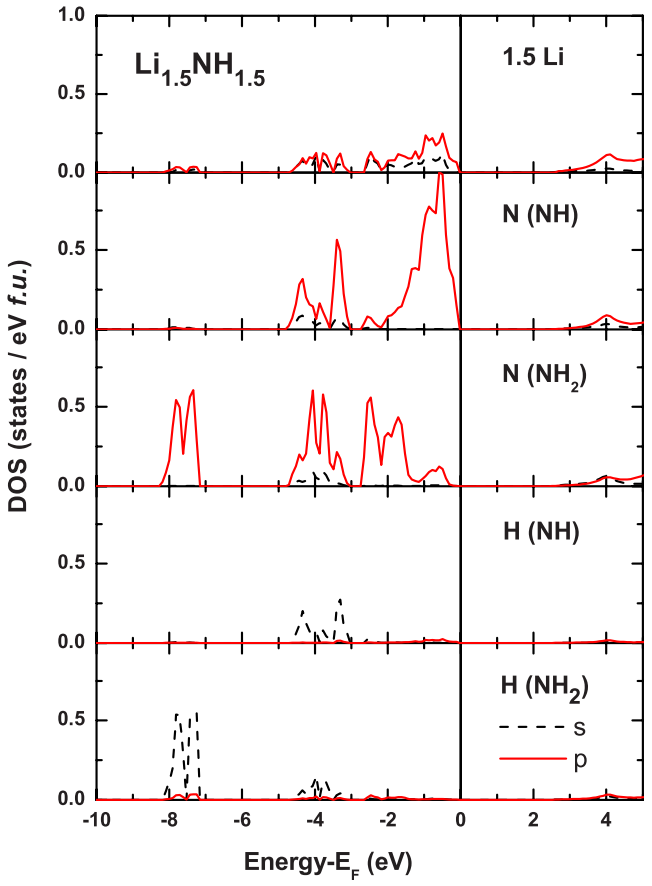

FIG. 7. (Color online) Partial wave analysis of the density of states of $Li_{1.5}NH_{1.5}$ around the atomic sites (*s* states: dashed line, *p* states: full line).

and as well for Li_4NH, the Bader charges are about +0.8 on Li, −2.4 on N, and −0.8 on H atom, indicating a strong ionic character for these compounds. For the $Li_{2-x}NH_{1+x}$ ($x=0,0.5,1$) compounds, the charge on Li is still about +0.8 but the anionic contribution is now shared by two kind of entities $[NH]^{2-}$ and $[NH_2]^-$: in Li_2NH, charge on NH is −1.65 whereas in $LiNH_2$, charge of NH_2 is −0.85. Like it was observed in the DOS analysis, a mixing of these two entities is found in $Li_{1.5}NH_{1.5}$ compound.

Figure 8 shows the valence-charge electronic localization function (ELF) calculated for Li_4NH and $Li_{2-x}NH_{1+x}$ ($x=0,0.5,1$) compounds. The ELF (Refs. 45 and 46) gives account of the type of bonding, it is defined as

$$\mathrm{ELF} = \frac{1}{1+\chi^2(r)}, \quad \chi(r) = \frac{D(r)}{D_{gas}(r)}$$

with

$$D(r) = \sum_i |\nabla \Psi_i(r)|^2 - \frac{1}{4}\frac{|\nabla \rho(r)|^2}{\rho(r)}$$

$$D_{gas}(r) = \frac{3}{5}(6\pi^2)^{2/3}\rho^{5/3}(r),$$

where $\rho(r)$ is the electron spin density and $\Psi_i(r)$ the spin orbital of occupied i state. In this way, Becke and Edgecombe[45] associated the localization of an electron with the probability density to find a second like-spin electron near the reference point. The smaller this probability density, i.e., the smaller the expression $D(r)$. The ELF has values between 0 and 1, where the value 1 corresponds to perfect localization, 0.5 indicates electron-gaslike probability $[D(r)=D_{gas}(r)]$, and values bellow 0.5 characterize regions of low electronic density. From the low values of ELF in the interatomic region between Li and the N-H cages, we conclude that the interaction between Li ions and N-H entities is dominantly ionic for Li_2NH, $Li_{1.5}NH_{1.5}$, and $LiNH_2$. As expected from the electronic band structure analysis, the Li_4NH phase does not present strong bonding between H and N, with localized electrons around the interstitial hydrogen atoms. In contrast, the $Li_{2-x}NH_{1+x}$ compounds present an increase in the charge density around $[NH]^{2-}$ and $[NH_2]^-$ entities with increasing x values ($x=0,0.5,1$), which comes along with a progressive ordering of $[NH_2]^-$ ions.

TABLE III. Average ionic radii and Bader charges of various compounds studied in this work, with PBE functional calculations. For $Li_{1.5}NH_{1.5}$ compound, the N and H atoms belonging, respectively, to $[NH]^{2-}$ and $[NH_2]^-$ entities are labeled as 1 and 2.

Compound	Atom or entity	Radius (Å)	Charge
Li_3N	Li	0.969	0.803
	N	1.993	−2.410
Li_4NH	Li	0.947	0.813
	N	1.872	−2.344
	H	1.591	−0.908
Li_2NH	Li	0.936	0.825
	N	1.749	−1.861
	H	1.056	0.211
	$[NH]^{2-}$		−1.650
$Li_{1.5}NH_{1.5}$	Li	0.941	0.836
	N1	1.773	−1.824
	N2	1.684	−1.475
	H1	1.037	0.204
	H2	0.996	0.290
	$[NH]^{2-}$		−1.620
	$[NH_2]^-$		−0.895
$LiNH_2$	Li	0.940	0.847
	N	1.707	−1.503
	H	1.016	0.328
	$[NH_2]^-$		−0.847
LiH	Li	0.949	0.830
	H	1.447	−0.830

V. ENTHALPIES OF FORMATION AND REACTIONS

The enthalpies of formation of the compounds entering in the hydrogenation process of Li_3N calculated with respect to H and N in their molecular forms and Li in its metallic state, defined by the following equation, are shown in Table IV,

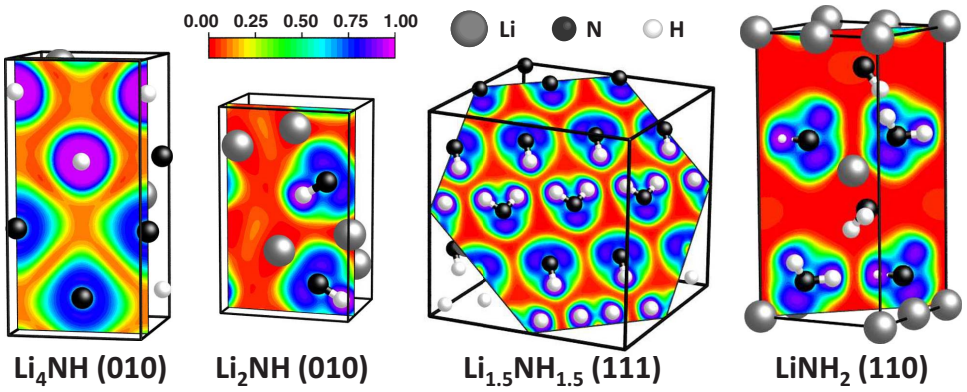

FIG. 8. (Color online) Valence-charge electronic localization function (ELF) calculated for Li_4NH and $Li_{2-x}NH_{1+x}(x=0,0.5,1)$ compounds. $Li_{1.5}NH_{1.5}$ is shown in a relaxed $2\times2\times2$ supercell model.

$$\Delta H_{formation}(Li_xN_yH_z) = E(Li_xN_yH_z) - xE(Li) - \frac{y}{2}E(N_2) - \frac{z}{2}E(H_2).$$

As expected, the results with the PBE, PBEsol functionals are somewhat different. Nevertheless, the physical interpretation concerning the phases' formation is unchanged. The ZPE contributions at 0 K are also shown. Since the ZPE have already been obtained by other authors[20,22,24,25,48] for most of the compounds using full phonon DOS calculations, we presently used these values. For the new phases, an estimate of the H-vibration contribution using a simple Einstein model has been considered. Table IV shows that both Li_4NH and $Li_{1.5}NH_{1.5}$ can be readily formed from the starting elements since their formation energies are highly negative. These formation enthalpies, however, do not provide clues regarding their actual formation during the hydrogenation reaction of Li_3N. In Table V, we have considered various possibilities for their formation.

As suggested by x-ray and neutron diffractions,[14] we first consider a possible decomposition of Eq. (1) with the two following steps:

$$2\ Li_3N + H_2 \Leftrightarrow Li_4NH + Li_2NH, \quad (3)$$

$$Li_4NH + H_2 \Leftrightarrow Li_2NH + 2\ LiH. \quad (4)$$

From Table V, we see that the direct reaction of Li_3N with H_2, as shown in Eq. (3), can lead to the formation of the compound Li_4NH with a very large exothermic enthalpy of formation, -148.92 kJ mol^{-1} H_2, larger than that for Li_2NH, -113.51 kJ mol^{-1} H_2, of Eq. (1). The products resulting from Eq. (3) are Li_4NH and Li_2NH. Indeed, the presence of this latter compound as a reaction product suggests that this highly exothermic enthalpy of formation of reaction (3) might not be entirely due to the formation of the compound Li_4NH. The reaction (3) can be considered to be a two step process involving reaction (1) which is a standard process, and reaction (7) of Table V, in which LiH obtained in reaction (1) reacts with Li_3N to form Li_4NH. The electronic contribution of reaction (7) is hardly favorable for this reaction

TABLE IV. Enthalpies of formation, ΔH_f (kJ mol^{-1}) of various compounds involved in the hydrogenation reaction with respect to the elements in their ground states: metallic Li, H_2, and N_2. The ZPE contributions (kJ mol^{-1}) are shown from our present calculations and from another theoretical work (Ref. 24). The column ΔH_f^{TOTAL} is the total contribution of ΔH_f^0 and E_{ZPE}. The negative sign indicates binding. For comparison, enthalpies of formation calculated with PBE and PBEsol functionals are also given.

	PBE	PBEsol	Calculated PW91				Expt.
	ΔH_f^0	ΔH_f^0	ΔH_f^0	E_{ZPE}	E_{ZPE} (Ref. 24)	ΔH_f^{TOTAL}	ΔH_f^{exp}
H_2				22.51	25.9		
NH_3	−102.09	−122.51	−102.58		87.70	−14.88	
Li_3N	−150.69	−161.19	−163.26		27.40	−135.86	−197[a]
Li_2NH $F\bar{4}3m$	−161.04	−148.02	−172.69				−222[a]
Li_2NH *Pnma*	−197.53	−218.01	−207.17	30.26	46.80	−160.37	−222[a]
$LiNH_2$	−186.18	−222.07	−204.32	50.00	69.30	−135.02	−176[a]
LiH	−79.73	−85.71	−84.60		21.50	−63.10	−91[a]
Li_4NH	−231.18	−248.87	−248.10	13.73		−234.37	
$Li_{1.5}NH_{1.5}$	−186.50	−208.47	−194.76	43.13		−151.63	

[a]Reference 47.

TABLE V. Enthalpies of various reactions, ΔH_r (kJ mol^{-1}). The negative sign indicates an exothermic reaction.

		PBE	PBEsol	Calculated PW91			Expt.
		ΔH_r^0	ΔH_r^0	ΔH_r^0	E_{ZPE}	ΔH_r^{TOTAL}	ΔH_r^{exp}
(1)	$Li_3N+H_2 \rightarrow Li_2NH+LiH$	−126.56	−142.53	−128.51	15.00	−113.51	−161[a]
(2)	$Li_2NH+H_2 \rightarrow LiNH_2+LiH$	−68.38	−89.77	−81.75	18.10	−63.65	−45 [a], −51[b]
(3)	$2\ Li_3N+H_2 \rightarrow Li_2NH+Li_4NH$	−127.32	−144.51	−128.75	−20.17	−148.92	
(4)	$Li_4NH+H_2 \rightarrow Li_2NH+2\ LiH$	−125.80	−140.56	−128.28	50.17	−78.11	
(5)	$2\ Li_2NH+H_2 \rightarrow 2\ Li_{1.5}NH_{1.5}+LiH$	−57.67	−66.64	−59.77	−11.74	−71.51	
(6)	$2\ Li_{1.5}NH_{1.5}+H_2 \rightarrow 2\ LiNH_2+LiH$	−79.08	−112.91	−103.74	47.94	−55.80	
(7)	$Li_3N+LiH \rightarrow Li_4NH$	−0.76	−1.97	−0.23	−35.17	−35.41	
(8)	$Li_2NH+LiNH_2 \rightarrow 2\ Li_{1.5}NH_{1.5}$	10.70	23.14	21.99	−29.84	−7.86	
	Reactions involving ammonia						
(9)	$4\ Li_3N+3H_2 \rightarrow 3\ Li_4NH+NH_3$	−192.87	−224.38	−193.83	−58.42	−252.25	
(10)	$4\ Li_3N+2\ H_2 \rightarrow 2\ Li_4NH+2\ Li_2NH$	−254.65	−289.01	−257.49	−40.35	−297.84	
(11)	$2\ Li_2NH+H_2 \rightarrow Li_4NH+NH_3$	61.78	64.63	63.66	−18.07	45.59	
(12)	$Li_3N+2\ NH_3 \rightarrow 3\ LiNH_2$	−203.67	−260.00	−244.55	5.10	−239.45	
(13)	$Li_2NH+NH_3 \rightarrow 2\ LiNH_2$	−72.74	−103.62	−98.89	4.10	−94.79	−83.7[c]
(14)	$LiH+NH_3 \rightarrow LiNH_2+H_2$	−4.36	−13.84	−17.14	−14.00	−31.14	−49.9[d]
(15)	$Li_3N+NH_3 \rightarrow Li_2NH+LiNH_2$	−130.92	−156.38	−145.65	1.00	−144.65	
(16)	$3\ LiNH_2 \rightarrow 2\ Li_{1.5}NH_{1.5}+NH_3$	83.45	126.75	−120.88	−33.94	+86.94	

[a]Reference 8.
[b]Reference 13.
[c]Reference 12.
[d]Reference 49.

but there is a large exothermic contribution from ZPE. Due to this ZPE contribution, our calculations thus confirm the production of this compound as an intermediate product. The interesting thing about Li_4NH is that its hydrogenation enthalpy [see Eq. (4)] is less exothermic than that of Li_3N in the standard reaction (1), however, it is slightly more exothermic than the hydrogenation reaction energy [Eq. (2)] of Li_2NH.

We have also shown in Table V the reaction energies for the formation of Li_4NH with the evolution of ammonia. The reaction (9) suggests that this compound can be also formed with the release of ammonia since the reaction enthalpy is highly exothermic. This release of ammonia is not desired in fuel cell applications. A careful examination of reaction (9) shows that it involves two intermediate steps, reactions (10) and (11). The reaction (11) that governs the formation of ammonia is highly endothermic due to its high positive electronic contribution. The exothermicity of reaction (9) is only provided by the reaction of Li_3N with H_2 [reaction (10)], that does not involve ammonia. Thus these calculations show that production of ammonia cannot occur during the formation of this intermediate compound Li_4NH. In all cases, the hypothetical reactions (12)–(16) in Table V also show that ammonia, if present, will immediately react with other products to form amide and imide, The experimental observation of Hu and Ruckenstein[50] that ammonia reacts immediately with LiH and hence there is no gas release, is in agreement with our calculation [reaction (14) in Table V]. Minor amounts of ammonia production have been observed,[50–52] for example, in special experimental conditions when the Li_3N sample was previously exposed to air.[50] It should be mentioned however that our calculations concern either perfectly stoichiometric compounds or intermediate phases of specific compositions. Decomposition processes of the lithium amide in a continuous nonstoichiometric manner proposed, for example, by David *et al.*[15] are beyond the scope of the present calculations.

We now consider the formation of the second intermediate compound $Li_{1.5}NH_{1.5}$ discussed in the literature. In the same way of decomposition of Eq. (1) by Li_4NH in Eqs. (3) and (4), an easy proposition of the $Li_{1.5}NH_{1.5}$ formation mechanism may be the decomposition of Eq. (2) into the two following (5) and (6) reactions:

$$2\ Li_2NH + H_2 \Leftrightarrow 2\ Li_{1.5}NH_{1.5} + LiH, \tag{5}$$

$$2\ Li_{1.5}NH_{1.5} + H_2 \Leftrightarrow 2\ LiNH_2 + LiH. \tag{6}$$

The reaction (5) shows that this compound can be produced by the reaction of Li_2NH with H_2 with an enthalpy of reaction of −71.51 kJ mol^{-1} H_2. Again this reaction can be visualized as the sum of the standard reaction (2) with an exothermic energy of −63.65 kJ mol^{-1} H_2, and the reaction (8) in Table V. Since this latter presents a reaction energy which is exothermic (−7.86 kJ mol^{-1} H_2), reaction (5) is favored compared to Eq. (2). The formation of this intermediate compound $Li_{1.5}NH_{1.5}$ results from reaction (8) which is only slightly exothermic and owes its exothermicity largely to the

contribution from ZPE, that exceeds the endothermic electronic contribution.

Thus the proposed reactions involving the formation of intermediary phases Li_4NH and $Li_{1.5}NH_{1.5}$, and the absence of formation of ammonia, are in agreement with the experimental observations at 528 and 565 K by *in situ* x-ray powder diffraction in Ref. 16. Although the PBE and PBEsol functionals lead as expected to different numerical values of reaction enthalpies, the conclusions remain unaffected.

VI. CONCLUSIONS

We have performed DFT calculations to study the crystal structure, electronic structure, and stability of Li_4NH and $Li_{2-x}NH_{1+x}(x=0,0.5,1)$ compounds. For all these compounds, we optimized the atomic positions and lattice parameters with three exchange-correlation functionals. The structural results with these several functionals are quite similar and the calculated structures are in good agreement with the experimental results. Electronic band-structure studies reveal that all these compounds are insulators with a small band gap of about 2–3 eV.

While two intermediate compounds Li_4NH and $Li_{1.5}NH_{1.5}$ have been proposed experimentally, our calculations confirm that the formation of both compounds is possible during hydrogenation of Li_3N. The former with its hydrogenation properties is more favorable for dehydrogenation than the standard Eq. (1) and the formation of the second $Li_{1.5}NH_{1.5}$ is found to be favorable in comparison with the standard reaction (2).

The chemical bonding of hydrogen in the Li_4NH compound is, as expected, of different nature than in the other complex hydrides $Li_{2-x}NH_{1+x}$, in which strong covalent N-H interactions occur. In Li_4NH, the interaction of H-*s* state occurs only with Li *sp* states, as expected from the structural features. From the present DFT optimization, $Li_{1.5}NH_{1.5}$ is found to form in a cubic Li-vacant-type compound. Presently, the relaxed crystal structure of $Li_{1.5}NH_{1.5}$ appears to be described as an ordered phase for the most stable configuration, with coexistence of ordered $[NH]^{2-}$ and $[NH_2]^-$ anions in the same plane. The electronic structure of the $Li_{1.5}NH_{1.5}$ phase reveals clearly the presence of two distinct types of nitrogen atoms forming ordered imide and amide ionic entities in equal proportion. This feature confers to $Li_{1.5}NH_{1.5}$ $(x=0.5)$ the transition state between the "NH" disordered compound, Li_2NH $(x=0)$ and the "NH_2" ordered compound, $LiNH_2$ $(x=1)$.

ACKNOWLEDGMENTS

This work was performed using HPC resources from GENCI—CINES/IDRIS (Grants No. 2009-096175 and No. 2009-090189). We thank CINES (Centre Informatique National de l'Enseignement Supérieur) and IDRIS (Institut du Développement en Ressources Informatiques et Scientifiques) for providing us the computational facilities for performing the work presented in this paper.

*crivello@icmpe.cnrs.fr

[1] L. Schlapbach, *Topics in Applied Physics: Hydrogen in Intermetallic Compounds I* (Springer-Verlag, Berlin, 1988), Vol. 63.
[2] L. Schlapbach, *Topics in Applied Physics: Hydrogen in Intermetallic Compounds II* (Springer-Verlag, Berlin, 1988), Vol. 64.
[3] P. Dantzer, in *Interstitial Intermetallic Alloys*, edited by F. Grandjean, G. Long, and K. H. J. Buschow (Kluwer, Dordrecht, 1995), Chap. 7.
[4] P. Dantzer, Mater. Sci. Eng., A **329-331**, 313 (2002).
[5] A. Percheron-Guégan, in *Interstitial Intermetallic Alloys*, edited by F. Grandjean *et al.* (Kluwer, Dordrecht, 1995), Chap. 6.
[6] B. Bogdanović and M. Schwickardi, J. Alloys Compd. **253-254**, 1 (1997).
[7] A. Züttel, P. Wenger, S. Rentsch, P. Sudan, Ph. Mauron, and Ch. Emmenegger, J. Power Sources **118**, 1 (2003).
[8] P. Chen, Z. Xiong, J. Luo, J. Lin, and K. Tan, Nature (London) **420**, 302 (2002).
[9] T. Ichikawa, S. Isobe, N. Hanada, and H. Fujii, J. Alloys Compd. **365**, 271 (2004).
[10] Y. Kojima and Y. Kawai, J. Alloys Compd. **395**, 236 (2005).
[11] W. Luo, J. Wang, K. Stewart, M. Clift, and K. Gross, J. Alloys Compd. **446-447**, 336 (2007).
[12] P. Chen, Z. Xiong, J. Luo, J. Lin, and K. L. Tan, J. Phys. Chem. B **107**, 10967 (2003).
[13] W. Luo, J. Alloys Compd. **385**, 316 (2004); **381**, 284 (2004).
[14] E. Weidner, D. Bull, I. Shabalin, S. Keens, M. Telling, and D. Ross, Chem. Phys. Lett. **444**, 76 (2007).
[15] W. I. F. David, M. O. Jones, D. H. Gregory, C. M. Jewell, S. R. Johnson, A. Walton, and P. P. Edwards, J. Am. Chem. Soc. **129**, 1594 (2007).
[16] D. Chandra, R. Černý, D. Phanon, and N. Penin (unpublished).
[17] R. Niewa and D. A. Zherebtsov, Z. Kristallogr. - New Cryst. Struct. **217**, 317 (2002).
[18] S. Orimo, Y. Nakamori, G. Kitahara, K. Miwa, N. Ohba, T. Noritake, and S. Towata, Appl. Phys. A **79**, 1765 (2004).
[19] J. F. Herbst and L. G. Hector, Jr., Phys. Rev. B **72**, 125120 (2005).
[20] K. Miwa, N. Ohba, S. Towata, Y. Nakamori, and S. Orimo, Phys. Rev. B **71**, 195109 (2005).
[21] Y. Song and Z. X. Guo, Phys. Rev. B **74**, 195120 (2006).
[22] B. Magyari-Köpe, V. Ozoliņš, and C. Wolverton, Phys. Rev. B **73**, 220101(R) (2006).
[23] M. Gupta and R. P. Gupta, J. Alloys Compd. **446-447**, 319 (2007).
[24] A. R. Akbarzadeh, V. Ozoliņš, and C. Wolverton, Adv. Mater. (Weinheim, Ger.) **19**, 3233 (2007).
[25] L. G. Hector, Jr. and J. F. Herbst, J. Phys.: Condens. Matter **20**, 064229 (2008).
[26] W. Kohn and L. Sham, Phys. Rev. **140**, A1133 (1965).
[27] G. Kresse and J. Furthmüller, Phys. Rev. B **54**, 11169 (1996).
[28] G. Kresse and D. Joubert, Phys. Rev. B **59**, 1758 (1999).
[29] J. P. Perdew and Y. Wang, Phys. Rev. B **45**, 13244 (1992).

[30] J. P. Perdew, K. Burke, and M. Ernzerhof, Phys. Rev. Lett. **78**, 1396 (1997).
[31] J. P. Perdew, A. Ruzsinszky, G. I. Csonka, O. A. Vydrov, G. E. Scuseria, L. A. Constantin, X. Zhou, and K. Burke, Phys. Rev. Lett. **100**, 136406 (2008).
[32] H. Monkhorst and J. Pack, Phys. Rev. B **13**, 5188 (1976).
[33] P. E. Blöchl, O. Jepsen, and O. K. Andersen, Phys. Rev. B **49**, 16223 (1994).
[34] R. F. W. Bader, *Atoms in Molecules: A Quantum Theory* (Oxford University Press, New York, 1990).
[35] G. Henkelman, A. Arnaldsson, and H. Jónsson, Comput. Mater. Sci. **36**, 354 (2006).
[36] Bader charge analysis, http://theory.cm.utexas.edu/vtsttools/bader/
[37] K. Ohoyama, Y. Nakamori, S. Orimo, and K. Yamada, J. Phys. Soc. Jpn. **74**, 483 (2005).
[38] M. Sørby, Y. Nakamura, H. W. Brinks, T. Ichikawa, S. Hino, H. Fujii, and B. C. Hauback, J. Alloys Compd. **428**, 297 (2007).
[39] H. Jacobs and R. Juza, Z. Anorg. Allg. Chem. **391**, 271 (1972).
[40] T. Noritake, H. Nozaki, M. Aoki, S. Towata, G. Kitahara, Y. Nakamori, and S. Orimo, J. Alloys Compd. **393**, 264 (2005).
[41] M. P. Balogh, C. Y. Jones, J. F. Herbst, L. G. Hector, Jr., and M. Kundrat, J. Alloys Compd. **420**, 326 (2006).
[42] A. Rabenau and H. Schulz, J. Less-Common Met. **50**, 155 (1976).
[43] D. K. Smith and H. R. Leider, J. Appl. Crystallogr. **1**, 246 (1968).
[44] R. Marx, Z. Anorg. Allg. Chem. **623**, 1912 (1997).
[45] A. D. Becke and K. E. Edgecombe, J. Chem. Phys. **92**, 5397 (1990).
[46] B. Silvi and A. Savin, Nature (London) **371**, 683 (1994).
[47] *Gmelins Handbuch-Der Anorganischen Chemie*, edited by R. J. Meyer (Verlag Chemie GMBH, Weinheim, 1960), Vol. 20, pp. 273–270.
[48] K. J. Michel, A. R. Akbarzadeh, and V. Ozolins, J. Phys. Chem. C **113**, 14551 (2009).
[49] S. Hino, N. Ogita, M. Udagawa, T. Ichikawa, and Y. Kojima, J. Appl. Phys. **105**, 023527 (2009).
[50] Y. H. Hu and E. Ruckenstein, J. Phys. Chem. A **107**, 9737 (2003).
[51] G. Meisner, F. Pinkerton, M. Meyer, M. Balogh, and M. Kundrat, J. Alloys Compd. **404-406**, 24 (2005).
[52] T. Ichikawa, N. Hanada, S. Isobe, H. Leng, and H. Fujii, J. Phys. Chem. B **108**, 7887 (2004).